ELSEVIER

Journal of Applied Geophysics 49 (2002) 75–90

JOURNAL OF APPLIED GEOPHYSICS

www.elsevier.com/locate/jappgeo

ANN reconstruction of geoelectrical parameters of the Minou fault zone by scalar CSAMT data

V. Spichak [a,*], K. Fukuoka [b,1], T. Kobayashi [b], T. Mogi [c], I. Popova [a], H. Shima [d]

[a] *Geoelectromagnetic Research Institute, Troitsk, Moscow Region, Russia*
[b] *OYO Co., Tsukuba, Japan*
[c] *Institute of Seismology and Volcanology, Graduate School of Sciences, Hokkaido University, Sapporo, Japan*
[d] *OYO Co. U.S.A., San Jose, CA, USA*

Received 16 February 2000; accepted 2 February 2001

Abstract

Scalar controlled source AMT data collected in a northern part of the Minou fault area (Kyushu Island, Japan) are interpreted by means of the ANN Expert System MT-NET in terms of 3-D earth macro-parameters. A number of synthetic responses created in advance by means of forward modeling in typical 3-D geoelectrical models (conductive and resistive local bodies, fault, dyke, etc.) formed sequences for teaching an artificial neural network (ANN). MT-NET, once taught to the correspondence between the data images and the model parameters, is able to recognize unknown parameters given even incomplete and noisy data. The results of ANN reconstruction are compared with the resistivity distribution obtained for the same area using fast 3-D imaging based on synthesis of 1-D Bostick transforms of the apparent resistivities beneath each site as well as on 2-D TM mode inversion along four profiles. The best-fitting model reconstructed by ANN belongs to the guessed model class formed by ''dykes buried in the two-layered earth'', on the one hand, and to the equivalence class formed by all models giving rms misfit less than the noise level in the data, on the other hand.

Keywords: Scalar CSAMT; Three-dimensional interpretation; Artificial neural network; Occam inversion; Bostick transform; Fault

1. Introduction

Three-dimensional inversion of EM data in terms of a ''cell by cell'' conductivity distribution is a challenging problem both from theoretical and computational points of view. Many geophycisists hope that a breakthrough in this direction will enable them to solve practical problems, which require three-dimensional interpretation of incomplete and noisy data. However, in spite of recent achievements in 3-D inversion of synthetic MT fields by conjugate gradient technique (Mackie and Madden, 1993) and Bayesian statistics (Spichak et al., 1999b), it becomes evident that interpretation of real data requires a variety of tools to be used *depending* on the volume and quality of both the data and prior information available (Spichak, 1999a).

Unfortunately, application of methods mentioned above requires the geophysicist to know in advance 1-D layering and to supply an initial guess (expressed in deterministic or statistical terms) on the 3-D conduc-

* Corresponding author.
[1] Presently at Kyushu University, Japan.

0926-9851/02/$ - see front matter
PII: S0926-9851(01)00100-8

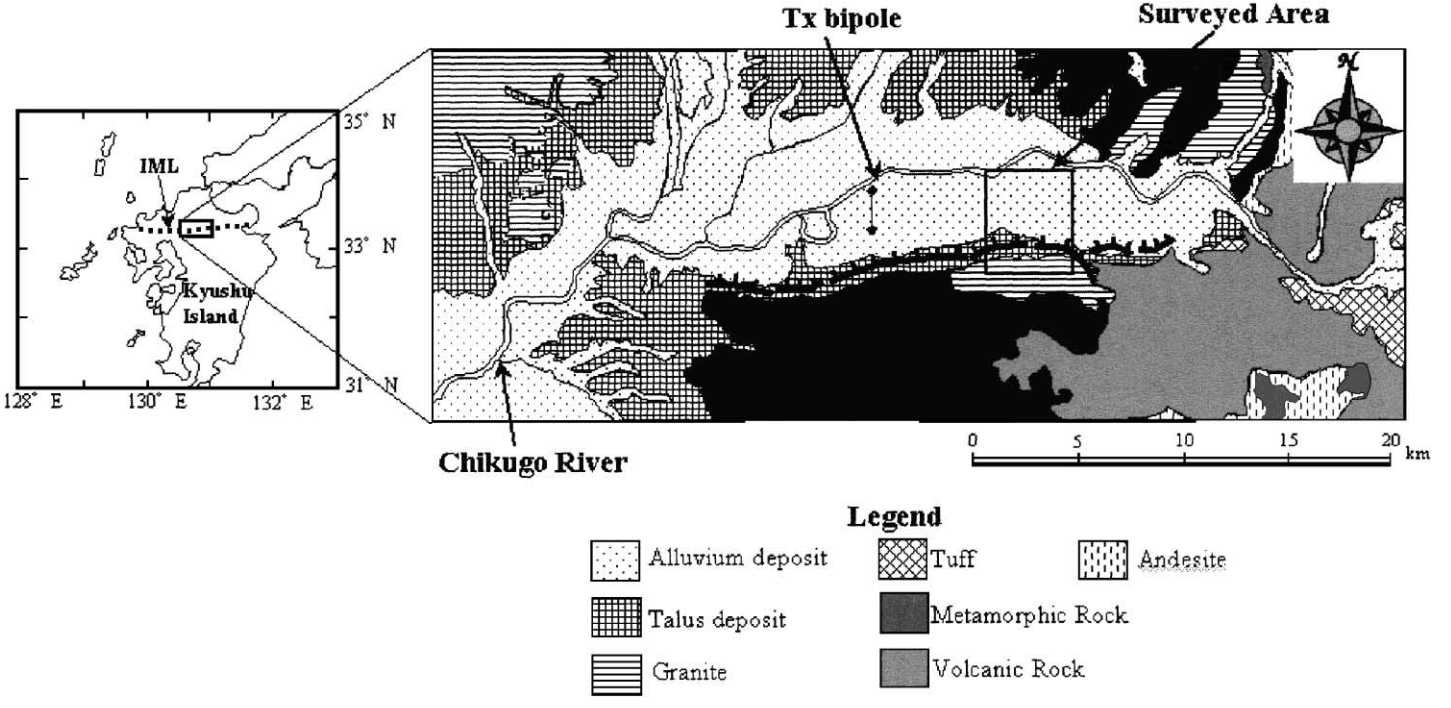

Fig. 1. Geological map of the Minou fault zone. The rectangle outlines the CSAMT survey area. IML—Imari–Matsuyama line.

tivity distribution in the region of search. Prior information comes often from other geophysical methods and we have to be able to incorporate it in a flexible way into the inversion procedure. On the other hand, sometimes geophysicists have only an idea about the *type* of unknown conductivity distribution (e.g., horst, graben, fault, etc.). In such a case, none of "regular" inversion techniques can transform EM data into a resistivity image.

An alternative approach especially useful in this situation could be developed in the framework of the artificial intelligence paradigm (see, for instance, Raiche, 1991). Hidalgo et al. (1994) and Poulton and Birken (1998) used Artificial Neural Networks (ANN) to determine the parameters of 1-D geoelectrical model, Poulton et al. (1992a,b) found the location of a two-dimensional target in a homogeneous half space, while Spichak and Popova (1998, 2000) reconstructed macro-parameters of a 3-D geoelectrical structure consisted from a fault buried in a two-layered earth.

The ANN approach does not require any prior information on the background geoelectrical section. It can be especially effective if the solution of the inverse problem is sought within a single class of models. Finally, ANN could be made insensitive to the prior knowledge on the noise level and used when the data are incomplete (Spichak et al., 1999a). The cost of these advantages is the time required for ANN's teaching, but, first, it could be done in advance and, second, once trained, ANN could be used then for interpretation of different data sets in terms of *known classes* of models (even under field conditions where data are noisy and incomplete).

The purpose of this study is to apply ANN Expert System MT-NET, developed and trained earlier (Spichak and Popova, 1998, 2000; Spichak et al., 1999a), to 3-D interpretation of scalar CSAMT data from a northern part of the Minou fault zone (Kyushu Island, Japan).

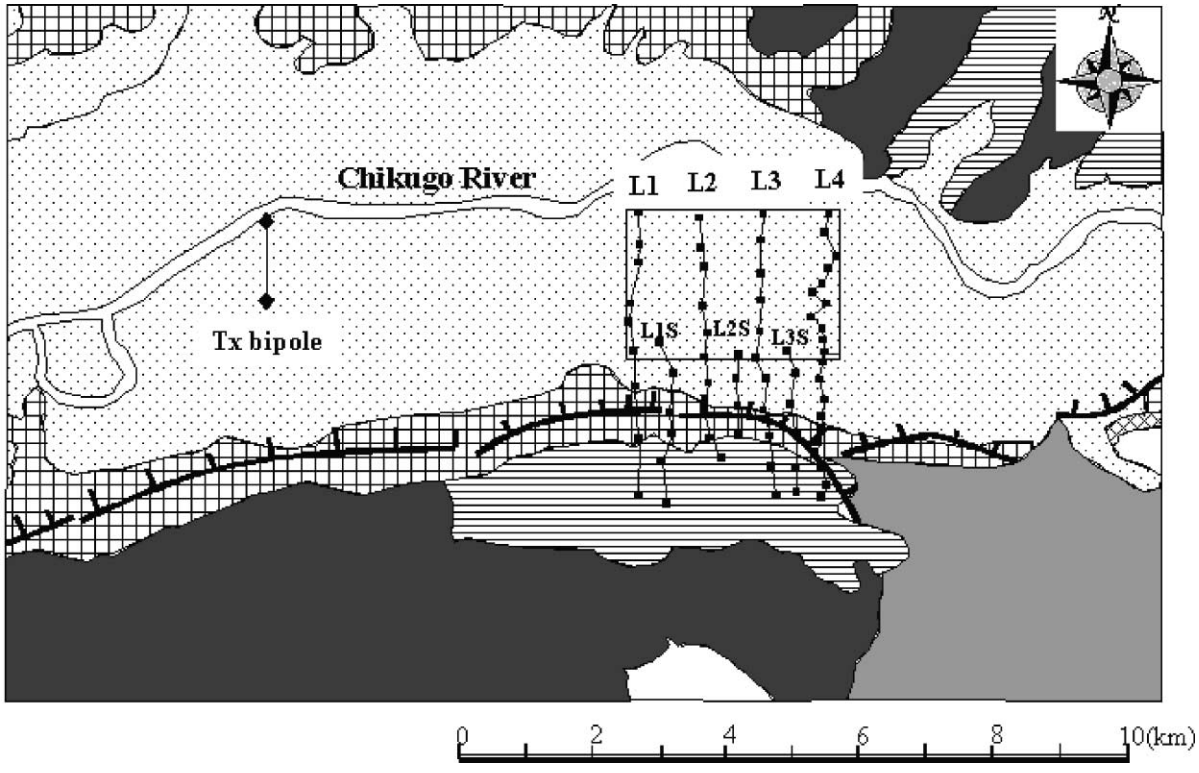

Fig. 2. Site location map (the rectangle defines the northern part of the Minou fault area). *Tx*—transmitter, L1–L4—survey lines.

2. Geological and geophysical setting

The Minou fracture zone is an active fault system and runs from the East to the West, North Kyushu, Southwest Japan (Chida, 1981). The Minou fault is one of the components of the Imari–Matsuyama Line (IML) situated at the boundary between the northern and central parts of Kyushu Island and is considered as a source of the great earthquake that occurred in 679 AD (Matumura, 1990). The fault runs on the northern foot of the Minou mountain range which is composed mainly from metamorphic rocks and located at the boundary between the mountain area and an alluvium plain extending along Chikugo river (Fig. 1).

A prominent low gravity anomaly is recognized at the northern side of the fault beneath the plain (Mogi et al., 1997). The anomaly extends to the East along the IML (Komazawa and Kamata, 1985). The depth to the metamorphic formation is decreased abruptly in the northern side of the fault and the maximum depth of it was estimated to be approximately 1.5 km (Mogi et al., 1997). This structure could be considered as a graben buried in a thick Quaternary sediment. The gravity and resistivity data revealed that the steep southern slope of the graben dipping northward is located 0.5–1.0 km to the north from the active fault line marked by the topographic discontinuity in the western part of the Minou fault zone (Mogi et al., 1997). At the eastern part of the area an outcrop of the metamorphic rocks is observed, though the granite–metamorphic rock boundary is not clear.

No marked displacement of the basement was detected by the gravity and resistivity data measured above the presently active fault. It seemed to have been active at the southern wall of the graben before Alluvium deposition. The active part "moved" then

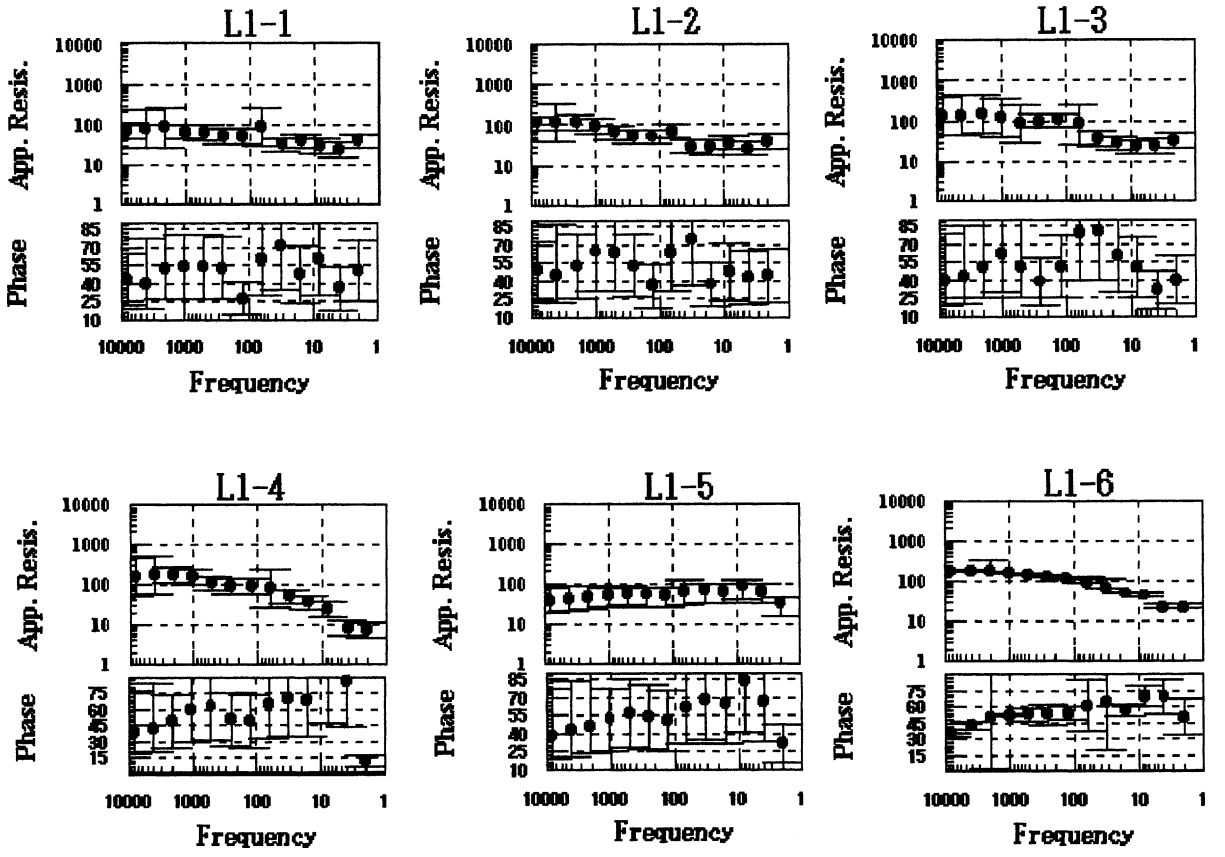

Fig. 3. Graphs of the apparent resistivities (in Ω m) and phases (in degrees) with standard errors versus frequency (in Hz) for the sites located along the profile L1.

to the south and a new activity has been started at the topographic discontinuity. This fault displacement suggests that extensional movement has been prevailing in this area during the Quaternary period.

Thus, the geology of the Minou fault zone is rather complicated and has to be studied by different methods. In particular, in order to determine the geoelectrical structure beneath the northern part of the Minou area a scalar CSAMT survey was carried out. Another aim of the measurements was to examine the applicability of the CSAMT survey to the resolution of an inclined fault zone.

3. CSAMT data acquisition and processing

CSAMT data collection was arranged in four major measurement lines, which cover the surveyed area around the fault zone (Fig. 2). The transmitting bipole *Tx* was oriented in nearly North–South direction and located about 6 km away from the nearest profile L1.

In the northern part of the region (outlined by the rectangle in the Fig. 2) only scalar measurements were conducted, so the electric field *Ex* was measured in the North–South direction (parallel to the bipole) and the magnetic field *Hy* was recorded in the East–West direction. The measurement points were aligned at about 500 m intervals in each line. Along the profile L4, the intervals were reduced to 250 m and twice as many measurement points as along other profiles were placed.

The length of the *Tx* bipole was about 1.9 km. The transmitter used (model CH-97T, Chiba Electric Research, Japan) generally creates 9 kW output power. The contact with the ground was established by 100 copper electrodes at each end of the bipole. The

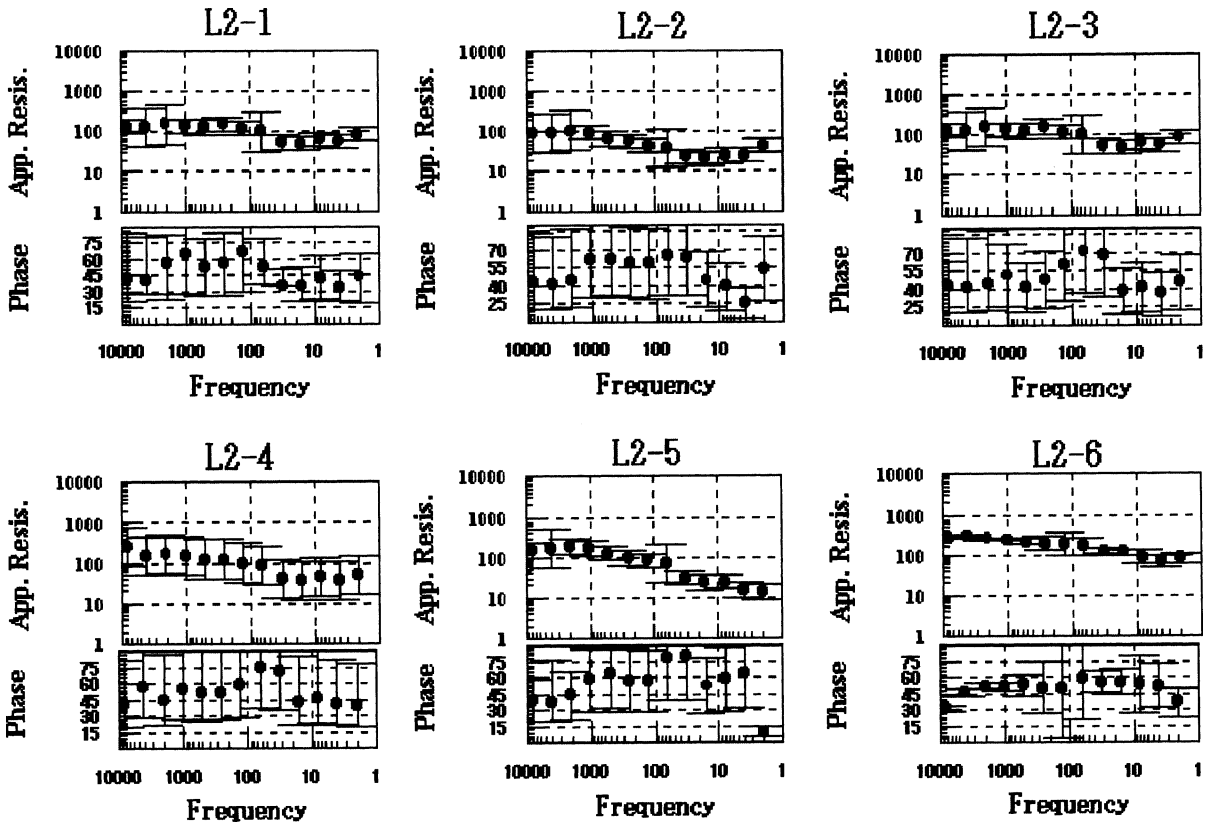

Fig. 4. Graphs of the apparent resistivities (in Ω m) and phases (in degrees) with standard errors versus frequency (in Hz) for the sites located along the profile L2.

impedance of the source was about 20 Ω between the two ends, so that a current of 15 A was achievable at lower frequencies. The frequency of acquisition ranged from 2 to 16,384 Hz in a binary progression.

The equipment used for scalar measurements was the MELIS system (IRIS Instruments, France). The frequency band of the MELIS system ranges from 1 Hz to 8 kHz. The receiver consists of two channels for measuring of one magnetic and one electric field components. MELIS calculates the discrete Fourier transform and power spectra of the time varying EM fields. The spectra are stacked then with the weights, which are calculated from the ratios between the power spectra at the measuring and contiguous frequencies. Thus, the data set at a certain frequency consists of the stacked power spectra of the electric and magnetic components and corresponding stacking weight.

Stainless rod electrodes were used for the electric field measurements, and CMS induction coils (IRIS Instruments) were used to measure magnetic field components. The characteristic response of the coil is flat over the frequency range used and the sensitivity is about 50 mV/nT.

Calculation of the apparent resistivities and phases in each site was carried out using weighting according to their coherencies followed by selective stacking by means of the "jacknife" procedure. Figs. 3–6 show apparent resistivities and phases for the sites located along profiles L1–L4, correspondingly. The quality of the collected data is fairly good, however, in the northern part of the surveyed area there were registered some data contaminated by cultural noise.

The behavior of the apparent resistivity and phase curves indicates that the geoelectrical structure of the northern part of the Minou fault zone could be

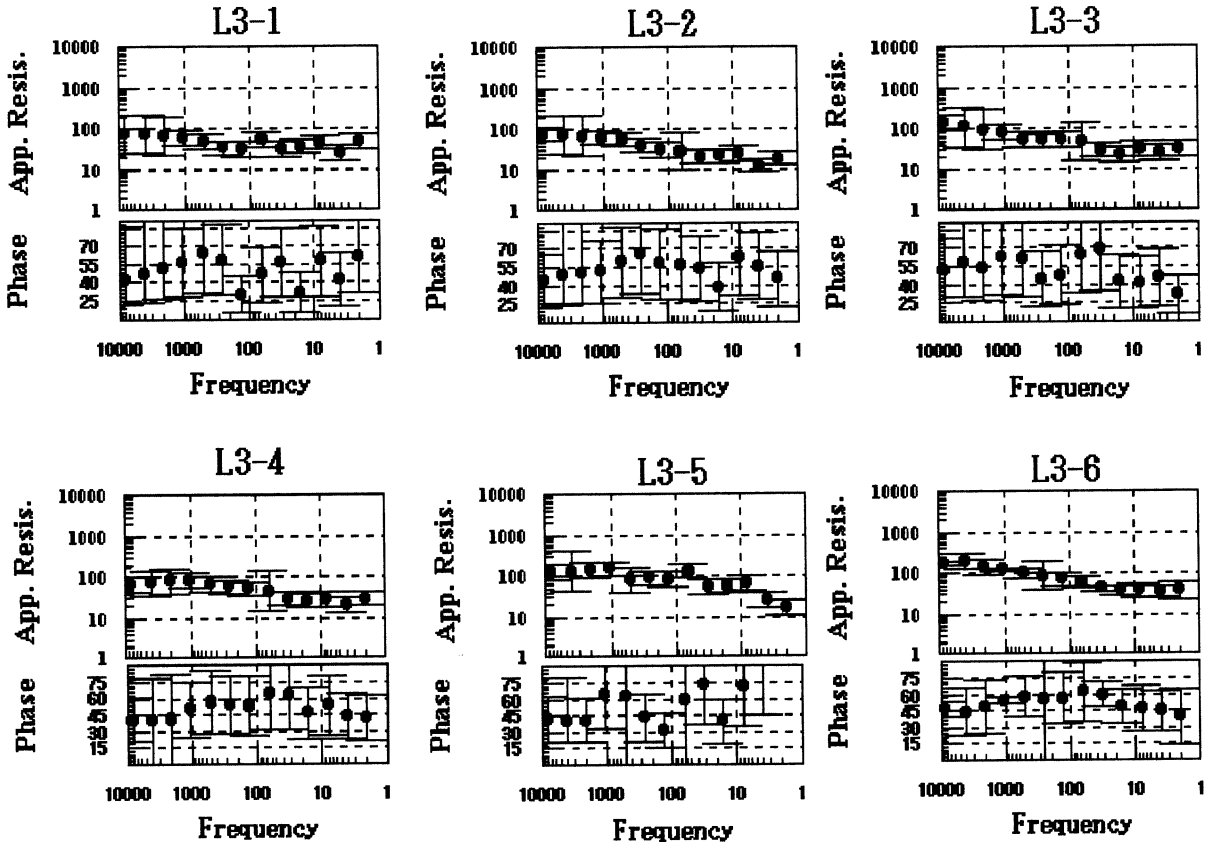

Fig. 5. Graphs of the apparent resistivities (in Ω m) and phases (in degrees) with standard errors versus frequency (in Hz) for the sites located along the profile L3.

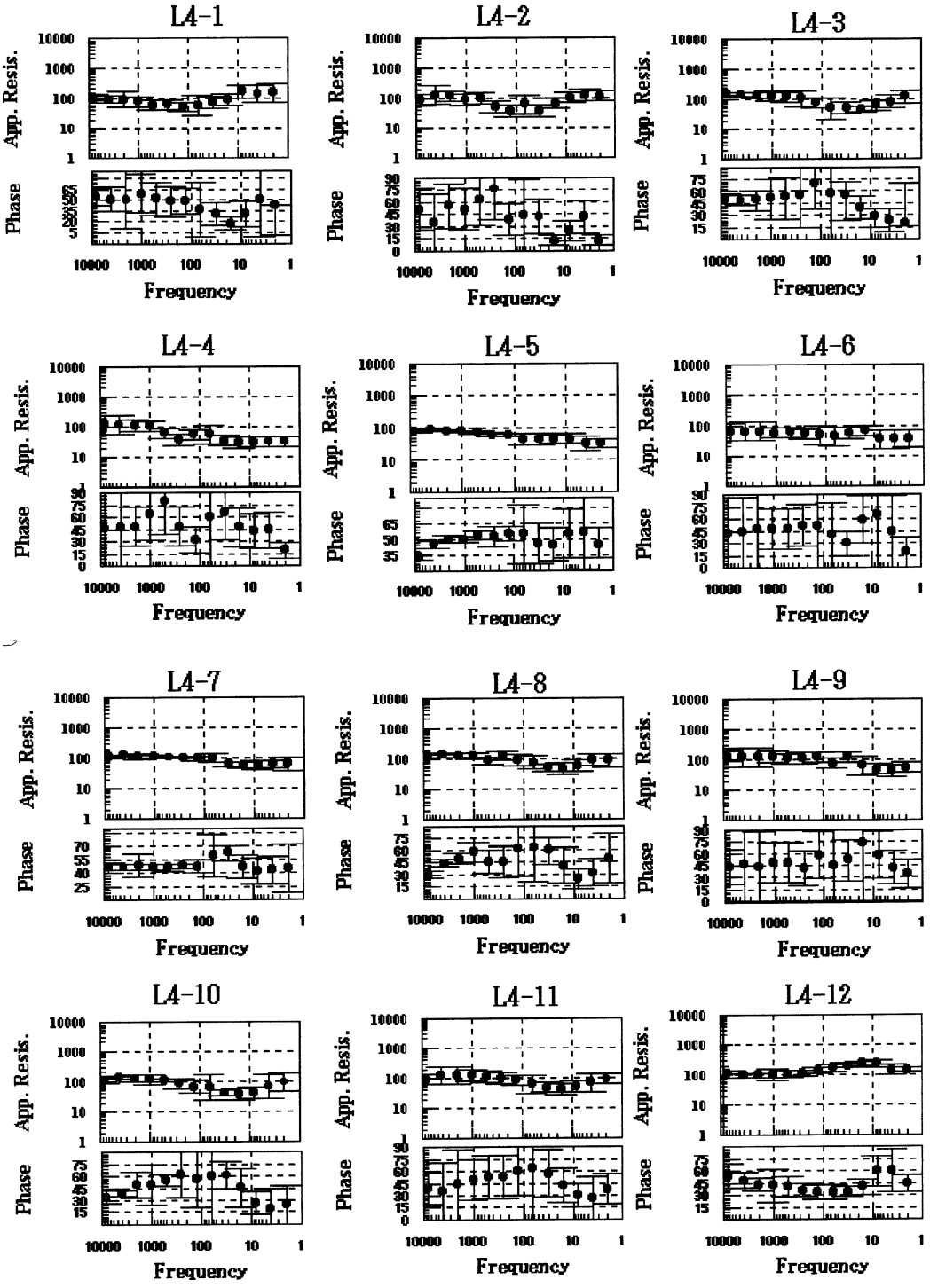

Fig. 6. Graphs of the apparent resistivities (in Ω m) and phases (in degrees) with standard errors versus frequency (in Hz) for the sites located along the profile L4.

considered as quasi horizontally layered with the resistivity of the first layer close to 100 Ω m. Another characteristic feature of the geoelectrical structure revealed by these figures is that the resistivity in the area between the profiles L1 and L3 slightly decreases with depth, so, a presence of relatively low resistive zone at some depth could be expected.

4. 3-D imaging based on synthesis of 1-D and 2-D inversion results

The interpretation of the data was carried out for frequencies higher than 8 Hz, so that the distance between the transmitter and the sounding locations was at least four skin-depths, which is far enough for a plane wave approximation of the source field and application of MT field equations. In order to get an idea about 3-D resistivity distribution in the northern part of the region basing on the scalar CSAMT data measured along profiles L1–L4 (Fig. 2) two independent ways of data inversion were used: (1) Bostick transforms beneath each site followed by 3-D synthesis of the results and (2) 2-D inversion along profiles.

4.1. Synthesis of Bostick transforms

It is often necessary to invert measured data when there is practically no prior information on the resistivity distribution in the area. In this case, the inversion methods based on usage of the prior data are not applicable. In this situation, it is useful for a preliminary estimation of the resistivity distribution to construct a three-dimensional *image* of the medium based on MT fields or their transforms

$$\tilde{F}_i(\vec{r},(z_{\mathrm{app}})_j) = \hat{T}F_i(\vec{r},\omega_j)(j=1,2,\ldots,N_\omega), \qquad (1)$$

here F_i are the components of MT-field measured at the surface at a series of frequencies; $\hat{T}$ is the transforming operator; $\tilde{F}$ is the field's transformation; $\vec{r}$ is the radius-vector of observation point; ω_j is the frequency ($j=1,2,\ldots,N_\omega$); $(z_{\mathrm{app}})_j$ is the apparent depth at frequency ω_j.

Note that if, for example, $\hat{T}F = \frac{1}{\mu_0\omega}|Z|^2$ (known as Bostick transformation), where Z is the impedance, then $\tilde{F}$ takes on the meaning of an apparent resistivity. At the same time, it is possible to imagine other transformations of the observed field which make no clear physical sense, but enable to get a focused image of the geoelectrical structure (Spichak, 1999b).

In order to get a 3-D image of the resistivity beneath the northern part of the Minou fault zone, we compiled Bostick transforms of the apparent resistivity component ρ^a_{xy} calculated beneath each site along profiles L1–L4 (outlined by the rectangle in Fig. 2) for 14 frequencies ranging from 8 Hz up to 16384 Hz in a binary progression.

Fig. 7 shows a volume apparent resistivity image constructed basing on synthesis of 1-D Bostick trans-

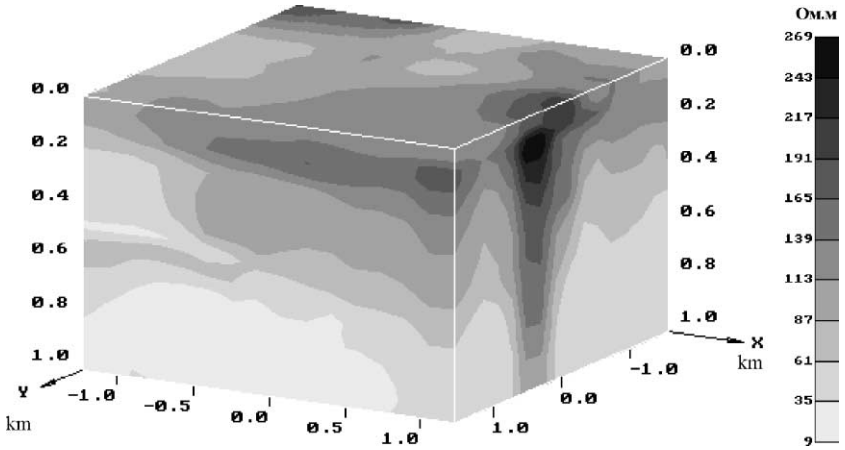

Fig. 7. Volume apparent resistivity image based on 3-D synthesis of Bostick transforms. (Axis Ox points in the North–South direction).

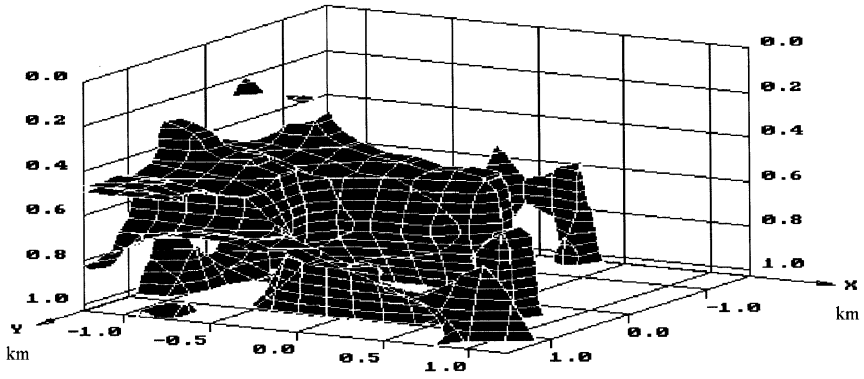

Fig. 8. Apparent resistivity isosurface ($\rho = 35\ \Omega$ m). (Axis Ox points in the North–South direction).

forms. It is seen that although the general 3-D resistivity distribution in the northern part of the Minou area is rather complicated, it has two features: first, the angle of inclination of the resistivity "layering" to the horizontal plane is approximately 20° and, second, the resistivity decreases downward so that a dipping low resistivity zone (resistivity less than 30 Ω m) beneath 500–800 m can be detected. Fig. 8 demonstrates explicitly the isosurface of the apparent resistivity equal to 35 Ω m. It is clear that the boundary between the relatively conductive and resistive zones lies at the depth about 500 m in the northern and at the depth about 800 m — in the southern part of the region.

Fig. 9 demonstrates vertical slices of the apparent resistivity in the *xOz* plane beneath each profile. The low resistivity zone (depth ~ 300 m, width ~ 200 m, length < 1000 m, angle of inclination ~ 30, resistivity < 30 Ω m) is seen here beneath the northern edge of the profile L2 (Fig. 9b).

4.2. 2-D inversion results

In order to construct a series of initial 2-D models, a multi-layered 1-D smoothness-constrained Occam's inversion of the apparent resistivity and phase data was first carried out for each site. The earth was considered to be composed of 50 artificial layers and their thicknesses were assumed to be known and fixed. The unknown resistivities of the layers were recovered using Tikhonov's regularization.

The results of 1-D inversions carried out beneath each site were then linearly interpolated in order to construct initial models for 2-D TM mode inversion along the profiles L1–L4 perpendicular to the fault strike direction. The finite element forward modeling

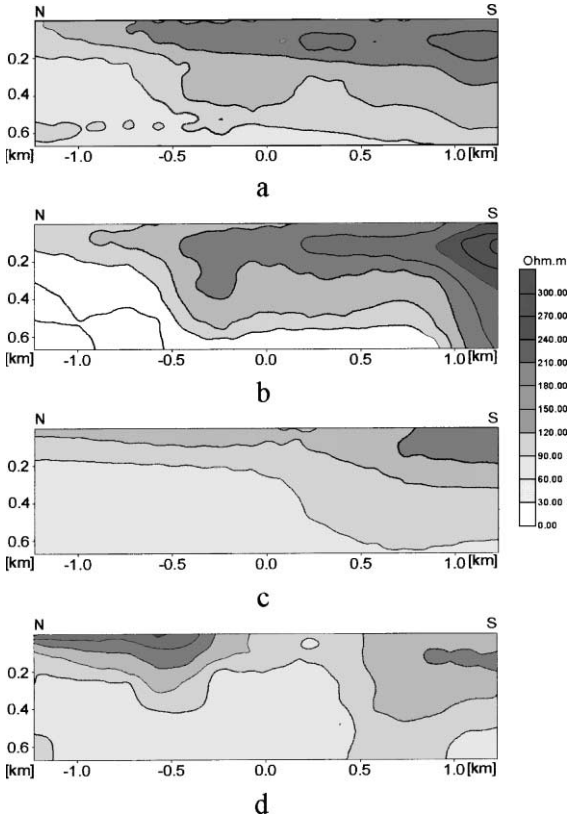

Fig. 9. Apparent resistivity cross-sections beneath profiles L1 (a), L2 (b), L3 (c) and L4 (d) based on syntheses of Bostick transforms.

and Powell's hybrid optimization technique (Powell, 1970) were used to refine the initial models in the framework of 2-D inversion procedure.

The low resistive zone detected earlier by synthesis of Bostick transforms is here more flat (Fig. 10): the depth at the northern part varies from 550 m at profiles L2 and L3 (Fig. 10b,c) to 850 m at profile L1 (Fig. 10a) the "dip angle" being around 10°. The low resistive zone, looking like a seam, (the resistivity contrast between the surrounding medium and the seam is approximately 2–5) has a width around 200 m, extends from the North to the South at a depth of approximately 600 m, lies mainly in the area beneath the profiles L1–L3 and is discontinuous beneath the profile L4.

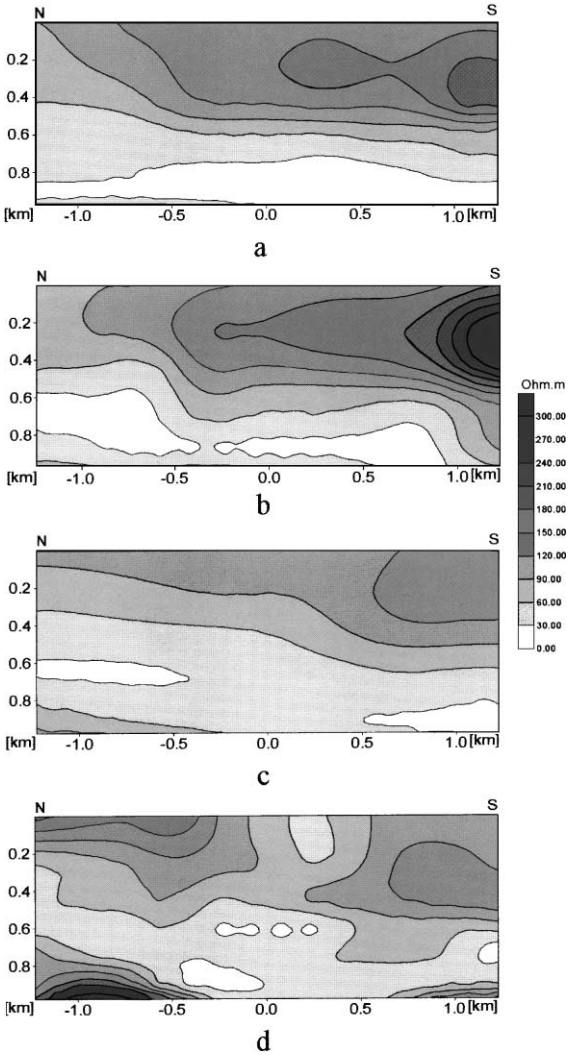

Fig. 10. Resistivity cross-sections beneath profiles L1 (a), L2 (b), L3 (c) and L4 (d) based on 2-D TM Occam's inversion.

5. ANN reconstruction of 3D geoelectrical structure

The previous section showed that 3-D imaging based on synthesis of 1-D Bostick transforms and 2-D inversion results reveal a relatively conductive seam dipping in the southern portion of the surveyed area. However, the resistivity image corresponding to the scalar CSAMT data can differ from the "true" 3-D resistivity distribution theoretically corresponding to more complete tensor CSAMT data that could be collected in this part of the Minou area. Moreover, a 3-D resistivity distribution resulting from synthesis of 1-D apparent resistivity transforms and 2-D inversion implicitly implies a local one-dimensionality of the medium beneath each site and two-dimensionality beneath each profile, respectively. Meanwhile, presentation of imaging (inversion) results using continuous function distributions independently of the quantity and quality of the data used gives a false impression that the number of degrees of freedom available is sufficient to determine tens or even hundreds of unknown model parameters. That is why alternative ways of model parameter reconstruction given insufficient and noisy data as well as adequate inversion results presentation (in particular, in terms of discrete parameters' values) are to be considered (Spichak et al., 1999a).

It is difficult to expect success in these directions within the framework of the well-known paradigm of geophysical data interpretation, which identifies it with the solution of a nonunique inverse problem. Instead we use one of the artificial intelligence techniques (ANN), which treats the data inversion as finding unknown model parameters based on a *similarity principle*. Application of this approach to the data inversion requires advance teaching of ANN using real or synthetic data and this process may take some hours of CPU (provided that appropriate data bases are already created). However, if the model class specified by the interpreter is already "familiar" to ANN (that is, ANN is already trained), reconstruction of the model parameters could be carried out practically instantaneously.

5.1. Neural network method of error backpropagation

We use a Neural Network Expert System MT-NET developed for 3-D interpretation of MT data in terms of earth macro-parameters (resistivities and thicknesses of the background layers, dimensions of the target, etc.) (Spichak and Popova, 2000). Its main element (ANN) is based on application of the "method of learning with a teacher", namely the error BackPropagation (BP) technique (see, for instance, Raiche, 1991). Such an approach to data inversion involves two stages: (1) training of a neural network, followed by (2) recognition of the model parameters (the inversion proper). At the training stage, the "teacher" specifies the correspondence between chosen input data and output variables. The functional elements of a biological neural system are similar to the nonlinear mapping "data → geoelectrical parameters" modeled by the artificial *n*-layered neural network, in which every neuron of one layer is connected to neurons of other layers. A signal arrives at the input layer of neurons from outside the system, whereupon its magnitude at the neurons of the other layers depends on the signal magnitudes and the connection coefficients of all neurons of the previous layer. Moreover, like in biological systems, the output response of an artificial neuron is described by a nonlinear function of the input signal.

MT-NET used for geoelectrical parameter reconstruction from CSAMT data is based on a three-layered ANN consisting of (1) a layer of input neurons (data), (2) a layer of hidden neurons, and (3) a layer of output neurons which are parameters of the geoelectric structure. Neurons of any two neighboring layers are connected so that the coefficients w_{ij} ("connection weights"), where i and j are the indexes of neurons of the two layers, determine the performance of the whole system.

The propagation of the input signal via such a network occurs in the following way. An input signal V_i^{inp} arrives at the ith neuron of the input layer for $i=1,\ldots,N_{\text{inp}}$. Each signal corresponds to the values of a measured electromagnetic field or its transformation. Every neuron of two other layers receives a summary input signal V_j^{inp} from all neurons of the previous layer,

$$V_j^{\text{inp}} = \sum_{k=l}^{N_{\text{pr}}} w_{k,j} U_k^{\text{out}}, \qquad (j = 1,\ldots,N) \tag{2}$$

where N and N_{pr} are the number of neurons in the considered and previous layers, accordingly; U_k^{out} is the output signal from the kth neuron of the previous layer, and the summation is carried out over all neurons of the previous layer. Each jth neuron of hidden or output layer transforms the input signal U_j^{inp} into U_j^{out} by the neuron response function G, defined by

$$U_j^{\text{out}} \equiv G(U_j^{\text{inp}}) \qquad (j = 1,\ldots,N) \tag{3}$$

where N is a number of neurons in the layer.

A mixed type (linear/nonlinear) of this function

$$G^{\text{mix}}(x) = 0.5 \cdot \begin{cases} (1+\tanh(x)), x < 0 \\ (1+x), x > 0 \end{cases} \tag{4}$$

was found in (Spichak and Popova, 2000) to be the most suitable for the problem considered. Thus, the output signal of the output layer is the result of processing the input signal through the various layers of the neural network.

At the training stage, we obtain the output signals U_i^{out} that minimize the standard error

$$\text{Er}_p = \sum_{i=1}^{N_{\text{out}}} (U_{i,p}^{\text{out}} - U_{i,p}^{t})^2 \qquad (p = 1,\ldots,N_p) \tag{5}$$

for each pth training sample; here N_p is the number of training samples, the summation is carried out over all neurons of the output layer (N_{out}), and $U_{i,p}^{\text{t}}$ is the value of the "correct" answer for this sample, which should correspond to the given input signal. This error is recorded for a single relation between input and output signals. Such "input–output" pairs are defined by the "teacher" and compose the training ANN sequence. The total standard error to be minimized is

$$\text{Er} = \sum_{p=1}^{N_p} \text{Er}_p, \tag{6}$$

where the summation is performed over all training samples. The connection coefficients of the input-hidden and hidden-output layers are the parameters that determine the signal propagation through the network and, therefore, the error value Er. Hence, the essence of the learning process is the search for

the matrix of neuron connections w_{ij} that minimizes the error (6) based on the teacher defined training sequence.

Learning starts from small (nonzero) random values of the connection coefficients. The input signal is propagated via network to the output layer. The output signal is then compared with the "correct" value, and the error is calculated. If the error exceeds some threshold value set by the "teacher", the signal is propagated back through the network to the input layer. The connection weights are set by the standard BP using the calculated error gradient at each step for each pair of neighboring layers and including an inertial term (contribution from the previous step) (see, for instance, Raiche, 1991)

$$\Delta w_{ij}^{(n)} = -\alpha \frac{\partial Er}{\partial w_{ij}} + \beta \Delta w_{ij}^{(n-1)}, \tag{7}$$

where $\Delta w_{ij}^{(n)}$ is the increment of the connection matrix at the nth iteration, $\Delta w_{ij}^{(n-1)}$ is its increment at the previous step, α is the rate of training, and β is the inertial coefficient ("learning momentum"), $0 < \beta < 1$. This procedure is fulfilled for the whole learning sequence and ends upon reaching a given accuracy threshold eps (Er < eps).

The inversion of real data uses the ANN interpolation and extrapolation properties. Unlike the training procedure requiring many steps of back and forth through-network movements of the signal, the inversion (recognition) procedure requires only one passage of the signal from the input to the output and uses the connection weights determined at the learning stage. Final values formed at the output layer are treated like they were the result of a data inversion constrained to a given model class.

5.2. ANN architecture

The architecture of the ANN used in this study (number of hidden layers and neurons, types of the gain functions, parameters α and β, etc.) was adjusted for its best performance in papers (Spichak and Popova, 1998, 2000). In particular, a comprehensive study was carried out aimed at finding the appropriate values of the following parameters of the ANN: types of activation function for hidden and output layers as well as for neurons at the output layer; number of neurons in a hidden layer; and the effect of a second hidden layer. Finally, a teaching precision was estimated which enabled reasonable inversion results to be obtained.

The ANN architecture was as follows: the input layer consisted of 80 neurons, the hidden layer consisted of 20 neurons, while the output layer consisted of six neurons, corresponding to the six model parameters to be recognized. The threshold level (eps) for rms errors in teaching was equal to 0.0075. The learning rate was equal to 0.01 and momentum to 0.9. In the process of teaching, the rms errors were used to estimate the misfits between the calculated and 'true' responses, so the total error for the test set for all parameters was determined as follows

$$\mathrm{Err} = \left[\frac{1}{N_{\mathrm{test}} N_{\mathrm{par}}} \sum_{n,j} \mathrm{err}_{n,j}^2 \right]^{1/2}, \tag{8}$$

where $\mathrm{err}(n, j) = [\mathrm{target}\ (n, j) - \mathrm{neural}\ (n, j)]/[\max(j) - \min(j)]$, $(j = 1, N_{\mathrm{par}};\ n = 1, \ldots, N_{\mathrm{test}})$; j is the number of the neuron in the output layer corresponding to the jth model parameter; n is the number of the tested sample; N_{par} is the number of the output neurons (=6); N_{test} is the number of the testing data sets; $\min(j)$, $\max(j)$—minimum and maximum values of jth parameter in the teaching pool, respectively; neural (n, j) is the recognition result for a jth parameter in nth testing sample; and target (n, j) is the target value of jth parameter in nth testing sample.

In order to estimate the quality of the ANN inversion of the synthetic data (when the true result was known in advance) for each jth unknown parameter the relative error averaged over all testing samples was calculated

$$\mathrm{Err}_j = \frac{1}{N_{\mathrm{test}}} \sum_{n} \frac{|\,\mathrm{target}_{n,j} - \mathrm{neural}_{n,j}\,|}{\mathrm{target}_{n,j}} \times 100\%. \tag{9}$$

5.3. Creation of the synthetic data base

In order for the ANN to learn the correspondence between the data and geoelectric parameters, it is first necessary to formulate the hypothesis on a class of inversion models, for instance dyke, geothermal res-

ervoir, magma chamber, oil or gas deposit, etc. (Note that we mean only the assumption on the *class of models* for which the solution is sought, rather than considerably more stringent constraints on the parameters of 1-D layering and/or target geometry used in the applications of other inversion methods.) This may be difficult in the general case, if we have no initial guess about the *type* of the geoelectric model to be searched for, but quite possible in some cases of practical importance.

The recognition of crustal dykes from the surface measurements of the electromagnetic field is an example of such a formulation of the problem. It is easily parameterized, and the inversion is reduced to the determination of a few macroparameters of the target itself as well as of the host medium. In particular, the following grading of unknown parameters was used in Spichak and Popova (1998, 2000) in order to create the synthetic data base for teaching ANN to be able to recognize the parameters of the dyke embedded in the two-layered earth (Fig. 11):

depth [D] = 50, 200 m;
conductivity of the first layer [C1] = 0.00333, 0.01 and 0.03 S/m;
conductivity of the second layer [C2] = 0.01 S/m (fixed);
conductivity of the dyke [C] = 0.0002, 0.001, 0.003333, 0.01, 0.02, 0.034, 0.06, 0.1, 0.17, 0.3 and 0.5 S/m;
width [W] = 16.65, 25, 50, 66.6, 100 and 200 m;

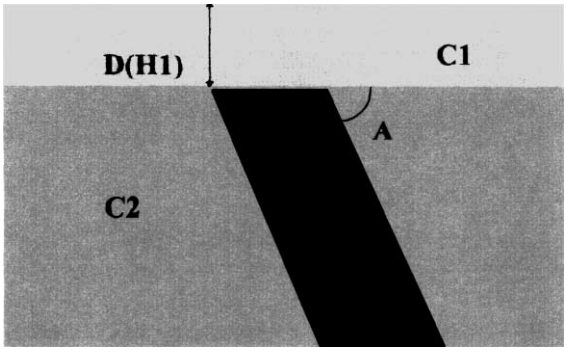

Fig. 11. Vertical cross-section of 3-D geoelectric model used for training ANN: C, C1 and C2 — conductivities of the dyke, first and second layer, respectively; D, W and A — depth, width and dip angle of the dyke, respectively.

length [L] = 16.65, 25, 50, 66.6, 83.25, 100, 125, 200, 250, 330, 500 and 1000 m;
angle of inclination [A] = 0°, 45°, 66°, 90°, 114°, 135° and 180°.

Note that due to restrictions on computation time, not all possible combinations of parameter values mentioned above were used for creation of the synthetic database. In particular, the total number of calculations was decreased by conditions like $D/W = 1, 2, 3$; $L/W = 1, 5$; 'basic' values of the conductivity contrast C/C2 = 2, 10, 50; and so on.

In order to reduce computation time (without loss of generality), the database used for teaching was smaller that the total one: only 90 synthetic data sets randomly selected from the total database were used. All calculations were carried out using the program package FDM3D (Spichak, 1983) for two primary field polarizations within the period range typical for audiomagnetotellurics: T = 0.000333, 0.001, 0.00333, 0.01, 0.0333 and 0.1 s. The total CPU time required for ANN training was less than 1 h (IBM PC, Pentium, 133 MHz).

5.4. ANN reconstruction of the Minou geoelectrical structure

According to the imaging and 2-D inversion results demonstrated in the previous sections, the geoelectrical structure of the northern part of the Minou fault zone was considered to be close to the model class of the type "dyke buried in a two-layered earth". So, we have applied the MT-NET taught in advance (Spichak and Popova, 1998) towards reconstruction of the geoelectrical parameters enumerated above basing on scalar CSAMT data collected in the northern part of the Minou area. Apparent resistivities ρ^{a}_{xy} and phases φ_{xy}; measured along profiles L1–L4 (see Figs. 3–6) for five frequencies (8, 32, 128, 256 and 1024 Hz) almost identical to those in the training data were used for ANN reconstruction. In order to eliminate the dependence of the ANN inversion results on the noise in the data a special pre-processing of the teaching samples was used (Spichak et al., 1999a).

In particular, we were interested in estimating the depth (D) to the upper edge of the target; the ratio (C1/C2) of the electrical conductivities of the first and second layers; ratio (C/C2) of the electrical conduc-

tivities of the target and hosting layer; width (W), length (L) and dip angle (A) of the target in the plane xOz (Fig. 11).

Table 1 shows the recognition results for two data sets used separately: apparent resistivities ρ^{a}_{xy} and phases φ_{xy} (data set 1) and only apparent resistivities ρ^{a}_{xy} (data set 2).

It is seen from the Table 1 that inversion of only apparent resistivities (data set 2) leads to underestimation (compared to the values obtained using data set 1) of all except two model parameters (C1/C2 and A). In other words, adding phases to the apparent resistivities changes the estimates of many model parameters, the biggest improvements being attributed to the first layer conductivity (from 6.59 to 0.36) and, to a less extent, to the dip angle (from 54° to 45°). It is worth mentioning in this connection that ANN reconstruction of the model parameters using *only* phases could give as precise results (at least, for synthetic data) as in the case of inversion of *both* apparent resistivities and phases (Spichak et al., 1999a). Thus, the following model parameters were determined by ANN: $RHO_1 = 100\ \Omega$ m, $RHO_2 = 36\ \Omega$ m, $RHO_t = 6\ \Omega$ m, D (H_1) = 310 m, $W = 390$ m, $L = 925$ m, $A = 45°$, where RHO_1, RHO_2 and RHO_t are the resistivities of the first and second layers, and the target, respectively.

5.5. Test of the ANN inversion result

In order to test the results of ANN recognition we have carried out the forward modeling by means of the same forward solver that was used for generation of the synthetic database. Electromagnetic fields for the model obtained using ANN were calculated for two polarizations of the primary field at six periods mentioned above.

The resulting apparent resistivities ρ^{a}_{xy} and phases φ_{xy} as well as observed data were interpolated then to the same rectangular grid with equal number of nodes in each direction (= 16) and the rms misfit was determined by the following formula

$$\Delta = \left\{ \frac{1}{2N_{xy}N_T} \left[\left\| \frac{\rho^{a}_{xy} - \tilde{\rho}^{a}_{xy}}{\delta\tilde{\rho}^{a}_{xy}} \right\|^2 + \left\| \frac{\varphi_{xy} - \tilde{\varphi}_{xy}}{\delta\tilde{\varphi}_{xy}} \right\|^2 \right] \right\}^{1/2}. \quad (10)$$

Here, N_T is the number of periods (= 6), N_{xy} is the number of interpolation points ($16 \times 16 = 256$), $\delta\tilde{\rho}^{a}_{xy}$ and $\delta\tilde{\varphi}_{xy}$ are standard deviations in apparent resistivity and phase, respectively, and the Euclidean norms are calculated as follows

$$\|f\| = \left[\sum_{i=1}^{N_{xy}} \sum_{j=1}^{N_T} |f(P_i, T_j)|^2 \right]^{1/2},$$

where P_i are the interpolation points.

The total rms misfit determined according to the formula (10) was equal to 0.91. (Note that the expected value of this misfit is equal to 1.0, which corresponds to the case, when the misfits in apparent resistivities and phases are equal to corresponding standard errors in the data.) This means that the best-fitting model reconstructed by ANN belongs to the guessed model class formed by "dykes buried in the two-layered earth", on the one hand, and to the equivalence class formed by all models giving rms misfit (10) less than 1.0, on the other hand.

Note that if we used for interpretation more "educated" ANN (or many ANNs taught in advance towards one type of models each), the misfit (0.91) could be, probably, further diminished. However, striving for this rms misfit may become less than the noise level in the data and may lead to unjustified overestimation of the data and, on the contrary, underestimation of the initial geophysicist's guess expressed in terms of the expected geoelectrical model type.

It is worth mentioning in this connection that the knowledge about the noise level in the data enables to use it as a stopping criterion in the framework of deterministic inversion methods that imply the rms misfit minimization procedure (see, for example, Mackie and Madden, 1993) or to incorporate it

Table 1
Results of ANN interpretation of the northern part of the Minou fault data (1 — ρ_{xy}, φ_{xy} were used both; 2 — ρ_{xy} only)

Data sets used	Depth (m)	C1/C2	Width (m)	Length (m)	C/C2	Angle (degrees)
1	308	0.36	386	925	5.92	45
2	263	6.59	330	800	3.40	54

explicitly into the inversion process (as in the context of the Bayesian probabilistic inversion; Spichak et al., 1999b). The ANN parameters' recognition, in distinction to the deterministic methods mentioned above, does not use the rms misfit minimization procedure, at least, in the framework of a single Backpropagation scheme (see Section 5.1), so, the only way to compare the appropriate misfit with the standard error in the data consists in forward modeling for the model parameters estimated by means of ANN.

6. Discussion

Thus, we have interpreted the data measured in the northern part of the Minou area using (1) 3-D imaging based on synthesis of 1-D Bostick transforms, (2) 2-D Occam's inversion carried out along four profiles, and (3) ANN recognition in terms of the macro-parameters. In doing so, we made the following assumptions on the character of the resistivity distribution in the domain of search: (1) local one-dimensionality, (2) two-dimensionality (no resistivity changes in the East–West direction), and (3) belonging to the model class of the type "an inclined dyke buried in a two-layered earth", respectively.

Comparison of the resistivity models reconstructed by means of first two techniques (see Figs. 9 and 10, respectively) reveals some common features of the geoelectrical structure of the northern part of the Minou fault zone. First, the resistivity decreases in the northern direction and from the surface to depth. Second, the layering of the geoelectrical structure is not horizontal with the dip angle being varied from 10° to 25° . Finally, a relatively conductive zone (with resistivity less than 30 Ω m) is detected in the domain beneath the profiles L1, L2 and L3 (Figs. 9b and 10a–c).

The ANN inversion of the same data set results, as was mentioned above, in a three-dimensional resistivity model of an inclined dyke buried in a two-layered earth (see row 1 of the Table 1): $RHO_1 = 100$ Ω m, $RHO_2 = 36$ Ω m, $RHO_t = 6$ Ω m, D $(H_1) = 310$ m, $W = 390$ m, $L = 925$ m, $A = 45°$.

3-D model parameters reconstructed by ANN differ from those estimated by means of 1-D and 2-D interpretation tools that do not take into account 3-D effects. Three-dimensionality of the resistivity distribution in the Minou area is well seen from the comparison of 2-D resistivity cross-sections beneath the profiles L1–L4 (Fig. 10). In particular, the "length" of the low resistive zone in the East–West direction determined by ANN (925 m) matches very well with its value that could be estimated visually from the Fig. 10a–c, taking into account that the distance between each neighbouring profiles is 450–500 m.

Finally, very recent studies in the Minou fault zone revealed a number of hot springs that delineate presumably a hot water reservoir manifested in AMT data as a low resistive zone.

7. Conclusions

ANN interpretation of scalar CSAMT data measured in a northern part of the Minou area was carried out and the resulting 3-D resistivity distribution was formulated in terms of six macro-parameters of an inclined dyke model. The model represents the northern dipping slope of a graben inferred by gravity anomaly in this part of the Minou fault zone (Mogi et al., 1997).

Comparison of the resulting resistivity images obtained by different interpretation techniques (Bostick transforms, Occam's 2-D inversion in TM mode, ANN recognition) indicates that ANN reconstruction of 3-D model macro-parameters gives appropriate results even if incomplete (for instance, scalar instead of tensor CSAMT) and noisy data are inverted.

The best-fitting model reconstructed by ANN belongs to the guessed model class formed by "dykes buried in the two-layered earth", on the one hand, and to the equivalence class formed by all models giving rms misfit less than the noise level in the data, on the other hand.

The ANN model parameters' reconstruction could be very effective when the geoelectrical model searched for is among the model classes used for MT-NET education. In this case fast 3-D interpretation of even incomplete and noisy data could be carried out in the field. Another promising field of MT-NET application consists in interpretation of the monitoring data, since in this case the ANN learns itself by real data and, therefore, no prior time-consuming forward modeling is required.

Finally, the studies provided demonstrate that CSAMT data (even incomplete and noisy) can resolve the parameters of the inclined fault zone. Further studies are to be carried out aimed at construction of a three-dimensional geoelectrical model of the entire Minou fault area using vector CSAMT data collected in the southern part of the this region.

Acknowledgements

This study was supported by grants received from the OYO (EM-95) and Russian Basic Research Foundation (99-05-64552). The authors are thankful to the OYO for providing the CSAMT data collected in a Minou fracture zone.

The authors acknowledge Dr. Art Raiche for his valuable remarks and the anonymous reviewer, whose remarks, comments, scientific questions and enormous editorial work enabled to improve greatly the manuscript.

References

Chida, N., 1981. Fault displacement topography at northern foot of the Minou mountain range, central Kyushu. Memoire of Fac. of Education, Iwate Univ. 40, 67–78 (in Japanese).

Hidalgo, H., Gomez-Trevino, E., Swinarski, R., 1994. Neural network approximation of an inverse functional. Proc. IEEE World Congr. on Computational Intelligence, 2715–3436, Orlando.

Komazawa, M., Kamata, H., 1985. Gravity basement structure in the Hohi area. Report Geol. Survey of Japan, No. 264, 305–333 (in Japanese with English abstract and figure captions).

Mackie, R.L., Madden, T.R., 1993. Three-dimensional magnetotelluric inversion using conjugate gradients. J. Geophys. 115, 215–229.

Matumura, K., 1990. Earthquake and Kamitu-Dorui ruins shown in the section of Tennmu-7 on the Nihon-Shoki. Kyushu Shigaku 98, 1–23 (in Japanese).

Mogi, T., Ehara, S., Nishijima, J., Motoyama, T., 1997. A graben structure at the western part of the Minou fault, southwest Japan. Jishin 50, 329–336 (in Japanese with English abstract and figure captions).

Poulton, M., Birken, R.A., 1998. Estimating one-dimensional models from frequency-domain electromagnetic data using modular neural networks. IEEE Trans. Geosci. Remote Sens. 36, 547–559.

Poulton, M., Sternberg, B., Glass, C., 1992a. Neural network pattern recognition of subsurface EM images. J. Appl. Geophys. 29, 21–36.

Poulton, M., Sternberg, B., Glass, C., 1992b. Location of subsurface targets in geophysical data using neural networks. Geophysics 57, 1534–1544.

Powell, M.J.D., 1970. A hybrid method for non-linear equations. In: Rabinowitz, P. (Ed.), Numerical Methods for Non-Linear Algebraic Equations. Gordon and Breach, London, pp. 87–161.

Raiche, A., 1991. A pattern recognition approach to geophysical inversion using neural networks. Geophys. J. Int. 105, 629–648.

Spichak, V.V., 1983. Program package FDM3D for numerical modeling of 3D-electromagnetic fields. In: Zhdanov, M. (Ed.), Algorithms and Programs for Solving Direct and Inverse Problems of EM-Induction in the Earth. IZMIRAN Publ., Moscow, pp. 58–68 (in Russian).

Spichak, V.V., 1999a. Magnitotellurichеskie polja v trekhmernikh geoelektricheskikh modeljakh (Magnetotelluric Fields in 3-D Geoelectric Models). Scientific World, Moscow (in Russian with English abstract).

Spichak, V.V., 1999b. Imaging volcanic interiors with MT data. In: Oristaglio, M., Spies, B. (Eds.), 3-D Electromagnetics. SEG Publ. (GD7), Tulsa, USA, pp. 418–425.

Spichak, V.V., Popova, I.V., 1998. Application of the neural network approach to the reconstruction of three-dimensional geoelectrical structure. Izvestiya, Phys. Solid Earth 34, 33–39.

Spichak, V.V., Popova, I.V., 2000. Artificial neural network inversion of MT-data in terms of 3D earth macro-parameters. Geophys. J. Int. 142, 15–26.

Spichak, V.V., Fukuoka, K., Kobayashi, T., Mogi, T., Popova, I., Shima, H., 1999a. Neural-network based interpretation of insufficient and noisy MT data in terms of the target macro-parameters. In: Zhdanov, M., Wannamaker, P. (Eds.), Extended Abst. 2nd Symposium on 3D Electromagnetics, Salt-Lake City, USA, pp. 297–300.

Spichak, V.V., Menvielle, M., Roussignol, M., 1999b. Three-dimensional inversion of the magnetotelluric fields using Bayesian statistics. In: Oristaglio, M., Spies, B. (Eds.), 3-D Electromagnetics. SEG Publ. (GD7), Tulsa, USA, pp. 406–417.